

Article

## Modularly Designed Peptide Nanoprodrug Augments Anti-Tumor Immunity of PD-L1 Checkpoint Blockade by Targeting Indoleamine 2, 3-Dioxygenase

Xuexiang Han, Keman Cheng, Ying Xu, Yazhou Wang, Huan Min, Yinlong Zhang, Xiao Zhao, Ruifang Zhao, Greg Anderson, Lei Ren, Guangjun Nie, and Yiye Li

*J. Am. Chem. Soc.*, **Just Accepted Manuscript** • DOI: 10.1021/jacs.9b12232 • Publication Date (Web): 16 Jan 2020

Downloaded from [pubs.acs.org](https://pubs.acs.org) on January 17, 2020

### Just Accepted

“Just Accepted” manuscripts have been peer-reviewed and accepted for publication. They are posted online prior to technical editing, formatting for publication and author proofing. The American Chemical Society provides “Just Accepted” as a service to the research community to expedite the dissemination of scientific material as soon as possible after acceptance. “Just Accepted” manuscripts appear in full in PDF format accompanied by an HTML abstract. “Just Accepted” manuscripts have been fully peer reviewed, but should not be considered the official version of record. They are citable by the Digital Object Identifier (DOI®). “Just Accepted” is an optional service offered to authors. Therefore, the “Just Accepted” Web site may not include all articles that will be published in the journal. After a manuscript is technically edited and formatted, it will be removed from the “Just Accepted” Web site and published as an ASAP article. Note that technical editing may introduce minor changes to the manuscript text and/or graphics which could affect content, and all legal disclaimers and ethical guidelines that apply to the journal pertain. ACS cannot be held responsible for errors or consequences arising from the use of information contained in these “Just Accepted” manuscripts.

# Modularly Designed Peptide Nanoprodrug Augments Anti-Tumor Immunity of PD-L1 Checkpoint Blockade by Targeting Indoleamine 2, 3-Dioxygenase

Xuexiang Han<sup>†,‡,§</sup>, Keman Cheng<sup>†,§,#</sup>, Ying Xu<sup>†,#</sup>, Yazhou Wang<sup>†</sup>, Huan Min<sup>†</sup>, Yinlong Zhang<sup>†,‡</sup>, Xiao Zhao<sup>†,‡</sup>, Ruifang Zhao<sup>†,‡</sup>, Gregory J. Anderson<sup>^</sup>, Lei Ren<sup>§</sup>, Guangjun Nie<sup>\*,†,‡</sup> and Yiye Li<sup>\*,†,‡</sup>

<sup>†</sup>CAS Key Laboratory for Biomedical Effects of Nanomaterials and Nanosafety, CAS Center for Excellence in Nanoscience, National Center for Nanoscience and Technology, Beijing 100190, P.R. China

<sup>‡</sup>Center of Materials Science and Optoelectronics Engineering, University of Chinese Academy of Sciences, Beijing 100049, P.R. China

<sup>§</sup>Department of Biomaterials, Key Laboratory of Biomedical Engineering of Fujian Province, College of Materials, Xiamen University, Xiamen 361005, P.R. China

<sup>^</sup>QIMR Berghofer Medical Research Institute, Royal Brisbane Hospital, Brisbane, Queensland 4029, Australia.

**ABSTRACT:** The limited efficacy of single-agent immune checkpoint inhibitors in treating tumors has prompted investigations on their combination partners. Here, a tumor-homing indoleamine 2, 3-dioxygenase (IDO) nanoinhibitor is reported to selectively inhibit immunosuppressive IDO pathway in the tumor microenvironment. It is self-assembled from a modularly designed peptide-drug conjugate containing a hydrophilic targeting motif (arginyl-glycyl-aspartic acid; RGD), two protonatable histidines and an ester bond-linked hydrophobic IDO inhibitor, which exhibits pH-responsive disassembly and esterase-catalyzed drug release. Markedly, it achieved potent and persistent inhibition of intratumoral IDO activity with reduced systemic toxicity, which greatly enhanced the therapeutic efficacy of programmed cell death-ligand 1 blockade *in vivo*. Overall, this study provides a promising paradigm of combinatorial normalization immunotherapy by exploiting a targeted IDO nanoinhibitor to augment the anti-tumor immunity of checkpoint inhibitors.

## INTRODUCTION

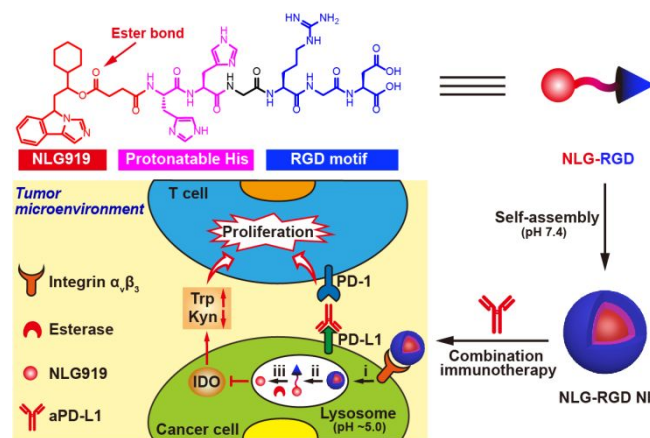
Immune escape is a fundamental characteristic during tumor growth and progression. Tumor cells exploit multiple mechanisms to evade host immune surveillance,<sup>1</sup> such as immune checkpoints, which refer to co-inhibitory receptors expressed on immune effector cells or immunosuppressive ligands expressed on tumor cells.<sup>2,3</sup> One of the best characterized immune checkpoint molecules is the programmed cell death-ligand 1 (PD-L1), which is up-regulated by malignant cells.<sup>4</sup> Ligation of PD-L1 to programmed cell death receptor (PD-1) expressed on T cells in the tumor microenvironment (TME) suppresses T-cell activation and proliferation.<sup>5</sup>

Correcting tumor-induced immune deficiency selectively in the TME to restore a natural anti-tumor immune capacity without severe systemic immune disorders is termed as normalization immunotherapy,<sup>6</sup> which has revolutionized the methodology of tumor therapy. In particular, immune normalization by targeting the PD-1/PD-L1 pathway holds great promise for regaining a lost anti-tumor immunity by restoring T cell activity.<sup>6,7</sup> In clinical trials, anti-PD-L1 antibody (aPD-L1) treatment induced durable tumor regression and prolonged stabilization of disease in various

malignancies.<sup>8</sup> However, only a small fraction of patients can benefit from this and the overall clinical efficacy of aPD-L1 monotherapy is still limited due to the existence of other immunosuppressive molecules in the TME.<sup>9,10</sup> Therefore, combinatorial normalization immunotherapy by concurrently blocking multiple pathways in the TME to boost the anti-tumor immune response of checkpoint inhibitor-based backbone therapy is widely regarded as the future of immunoncology.<sup>11-14</sup> Among various combination partners, indoleamine 2, 3-dioxygenase (IDO) inhibitors have great potential to enhance the efficacy of checkpoint blockade and are under active investigation in clinic.<sup>15-17</sup>

IDO is a cytosolic tryptophan-catabolizing enzyme that converts the essential amino acid L-tryptophan (Trp) to kynurenine (Kyn).<sup>18</sup> It is constitutively expressed in many tissues where it induces immune tolerance and prevents normal tissue injury.<sup>17</sup> Over-expression of IDO in tumor cells suppresses T-cell responses and recruits regulatory T (Treg) cells *via* Trp depletion and Kyn accumulation in the TME, leading to immune evasion and tumor growth.<sup>19,20</sup> Since IDO is an important target for immunotherapeutic intervention, several small molecule inhibitors are under clinical development,<sup>15</sup> including NLG919, a highly potent inhibitor.

However, as an imidazoleisoindole derivative, NLG919 suffers from poor water solubility and demands frequently high-dose administration to maintain IDO inhibition.<sup>17</sup> Furthermore, the nonspecific distribution of NLG919 and its strong potency can break IDO-mediated systemic immune balance and lead to severe adverse effects.<sup>16</sup>



**Scheme 1.** Schematic illustration of the modular design and self-assembly of NLG-RGD and the proposed mechanism of combinatorial normalization immunotherapy by concurrent blocking IDO and PD-L1 using NLG-RGD NI and aPD-L1. NLG-RGD NI is effectively internalized by cancer cells *via*  $\alpha_v\beta_3$  integrin receptor-mediated endocytosis (i) followed by acidic pH-triggered disassembly (ii) and esterase-catalyzed NLG919 release (iii).

To specifically normalize the Trp pathway in tumors and to avoid the shortcomings aforementioned, we develop a targeted IDO nanoinhibitor (denoted as NLG-RGD NI) based on a modularly designed, self-assembled peptide-drug conjugate NLG-RGD (Scheme 1), which shows the perfect integrity of structure and function: 1) RGD, a hydrophilic peptide, can achieve tumor targeting by binding to  $\alpha_v\beta_3$  integrin receptor; 2) Two histidines, a pH-recognizable moiety, can drive disassembly in the lysosome; 3) Ester bond, a hydrolysable linker, can achieve controlled drug release upon esterase treatment; 4) NLG919, a hydrophobic unit, can inhibit IDO activity. Compared to previously reported polymer-NLG919 nanoconjugates,<sup>10,21-24</sup> NLG-RGD NI consists of a biodegradable peptide backbone and a targeting motif with a drug loading content as high as 27% (Table S1). Moreover, the NLG-RGD NI greatly improves the bioavailability of NLG919 and exerts persistent inhibition of IDO activity with reduced systemic toxicity, which significantly boosts aPD-L1 based immunotherapy by reversing immune tolerance in both subcutaneous and orthotopic pancreatic tumor models.

## RESULTS AND DISCUSSION

**Synthesis and Characterization of NLG-RGD.** NLG-RGD was synthesized in two steps. First, a succinic acid-modified NLG919 (NLG-SA) was prepared (Figure 1A and Figure S1). Then, NLG-RGD was synthesized by a standard solid-phase peptide synthesis (SPPS) method using Fmoc protected amino acids and NLG-SA (Figure 1B). The

successful preparation of NLG-RGD was confirmed by analytical high performance liquid chromatography (HPLC, Figure 1C), matrix-assisted laser desorption ionization with time of flight mass spectrometry (MALDI-TOF-MS, Figure 1D) and Fourier transform infrared spectrometry (FT-IR, Figure S2).

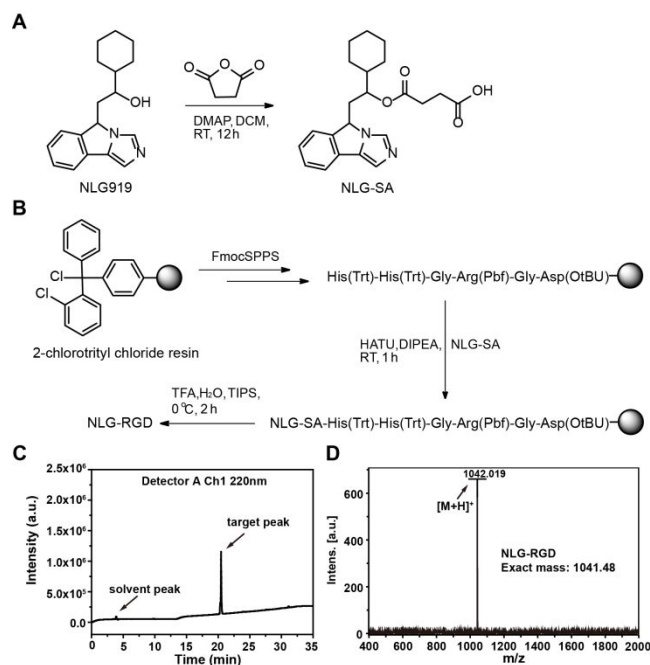


**Figure 1.** Synthesis and characterization of NLG-RGD. (A) Synthesis of NLG-SA. (B) SPPS synthesis of NLG-RGD. (C) HPLC trace of NLG-RGD. The purity of NLG-RGD is above 95%. (D) MALDI-TOF-MS analysis of NLG-RGD.

**Preparation and Characterization of NLG-RGD NI.** Due to the  $\pi$ - $\pi$  stacking and hydrophobic interactions, the amphiphilic NLG-RGD can self-assemble into NLG-RGD NI with a low critical micelle concentration (CMC, 2.63  $\mu$ M) (Figure S3). Transmission electron microscope (TEM) image revealed that NLG-RGD NI had a spherical morphology with a particle size of  $\sim$ 50 nm (Figure 2A), and its hydrodynamic diameter was  $\sim$ 70.2 nm with a surface charge of *ca.* -5.1 mV in neutral phosphate buffered saline (PBS, Figure 2B,C and Table S2). When pH was lowered to 6.5, NLG-RGD NI still maintained its spherical nanostructure (Figure S4). However, after pH dropped to 5.0, NLG-RGD NI quickly lost its structural integrity and become monomers or small aggregates in 2 h due to the disassembly driven by the protonated imidazole groups (Figure S5).<sup>25</sup> Meanwhile, its hydrodynamic size dropped to  $\sim$ 2.9 nm and surface charge increased to *ca.* 13.2 mV (Figure 2C).

The leakage of NLG919 from NLG-RGD NI was very slow without esterase (Figure S6A). However, upon esterase treatment, NLG-RGD NI displayed a sustained NLG919 release behavior at pH 7.4 or 6.5 and the release was obviously accelerated at pH 5.0 (Figure S6B-D and Figure 2D). This phenomenon can be explained by the increased accessibility between NLG-RGD monomer and esterase after the acidic pH-triggered structural dissociation. Such a

cooperatively responsive nanoinhibitor is supposed to prevent the premature release of NLG919 during its blood circulation, and enable the controlled release of NLG919 after engulfed into acidic lysosomes.

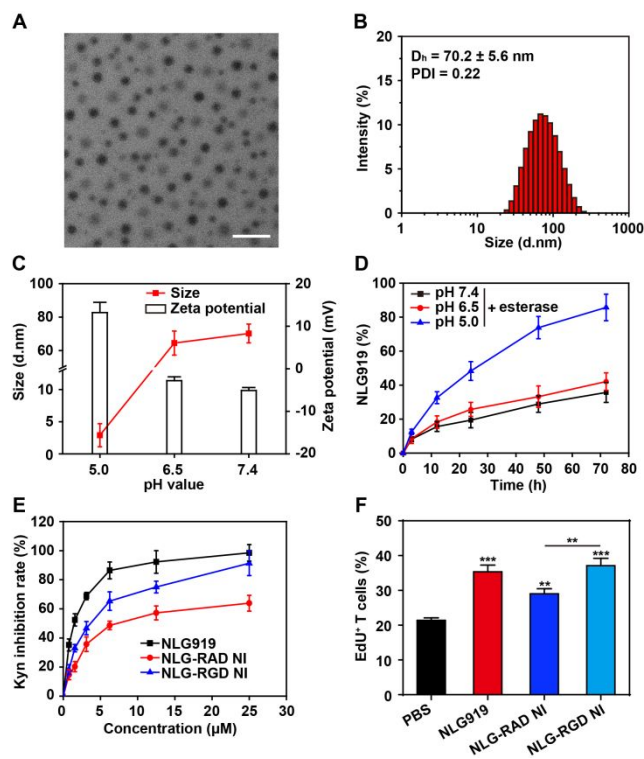


**Figure 2.** Preparation and characterization of NLG-RGD NI. (A) TEM image of NLG-RGD NI at pH 7.4. Scale bar, 200 nm. (B) The size distribution of NLG-RGD NI at pH 7.4. (C) Hydrodynamic size and zeta potential of NLG-RGD NI after equilibrium at pH 7.4, 6.5 or 5.0 for 2 h. (D) NLG919 release profile upon esterase treatment at different pHs. (E) IDO inhibition in Pan02 cells. (F) T-cell proliferation assay. Mean  $\pm$  SD.,  $n = 3$ . \*\* $p < 0.01$ , \*\*\* $p < 0.001$ , one-way ANOVA.

**IDO Inhibition *in Vitro*.** We then examined the cytotoxicity of NLG-RGD NI towards Pan02 cells. The result demonstrated that it had no influence on cell viability at concentration up to 100  $\mu$ M (Figure S7). Next, its capacity to block the conversion of Trp to Kyn was evaluated. For comparison, a non-targeted control nanoinhibitor (NLG-RAD NI) with similar physical properties was prepared by replacing glycine with alanine (Figure S8 and Table S2). NLG919 was a potent inhibitor of IDO activity, with a half maximum effect concentration ( $EC_{50}$ ) of 1.5  $\mu$ M (Figure 2E and Table S3). Its inhibition was dose-dependent in a narrow range of concentrations. NLG-RAD NI also showed dose-dependent inhibition, but over a wider range of concentrations and with a much higher  $EC_{50}$  (7.3  $\mu$ M) than NLG919. The reduced potency of NLG-RAD NI can be explained by requiring additional disassembly and hydrolysis steps to become its pharmacological active form. Notably, although NLG-RGD NI was less effective ( $EC_{50} = 3.9 \mu$ M) than NLG919, it had a stronger inhibitory effect on IDO activity than NLG-RAD NI presumably due to its enhanced cellular uptake.

To demonstrate that inhibition of IDO by NLG-RGD NI leads to enhanced T-cell proliferation, an *in vitro* T cells and Pan02 cells co-culture experiment was carried out.<sup>21,26</sup> NLG919 treatment led to a significant increase of EdU<sup>+</sup> T cells (Figure 2F and Figure S9), confirming the effectiveness of IDO blockade in stimulating T-cell proliferation. Notably, the proportion of EdU<sup>+</sup> T cells was also markedly elevated following NLG-RGD NI treatment. However, in line with its inferior inhibition of IDO activity, NLG-RAD NI exhibited moderate promotion of T-cell replication.

Next, we studied the cellular uptake behavior of nanoinhibitors. In order to track them, protoporphyrin IX-labeled peptides, PpIX-RGD and PpIX-RAD, were synthesized (Figure S10 and S11), and then were co-assembled with NLG-RGD and NLG-RAD to prepare PpIX-NLG-RGD NI and PpIX-NLG-RAD NI (Table S2), respectively. After incubation with Pan02 cells for 0.5 h, PpIX-NLG-RGD NI exhibited a stronger fluorescent signal than PpIX-NLG-RAD NI, confirming its more efficient cellular uptake (Figure S12A). Moreover, a highly co-localized fluorescence of PpIX and LysoTracker was observed in both groups, suggesting that these internalized nanoinhibitors were further transported to lysosomes. It is worth mentioning that lysosome is an acidic organelle (pH  $\sim$ 5) with abundant esterases,<sup>27</sup> which is in favor of cooperatively responsive NLG919 release. At 6 h post-treatment, a higher PpIX signal was still observed in PpIX-NLG-RGD NI treated cells and the fluorescence was mainly distributed in the cytoplasm, where the remaining prodrug molecules can be further hydrolyzed with the help of cytosolic esterases and the uncaged NLG919 can interact with IDO. The much higher cellular uptake of PpIX-NLG-RGD NI was also confirmed by flow cytometry (Figure S12B, C). It is identified that PpIX-NLG-RAD NI is preferentially taken up by clathrin-mediated endocytosis and the internalization of PpIX-NLG-RGD NI is mainly dependent on caveolae-mediated endocytosis (Figure S13), which are consistent with previous reported nanoparticles involved in RGD modification.<sup>28</sup> Together, these data suggest that RGD-mediated active targeting results in increased cellular uptake of NLG-RGD NI compared to NLG-RAD NI, finally leading to enhanced IDO inhibition.

**Pharmacokinetics and Pharmacodynamics.** Self-assembling peptide-drug conjugates are suggested to prolong the blood circulation of their hydrophobic cargo.<sup>29</sup> To prove this, a model hydrophobic molecule PpIX and PpIX-NLG-RGD NI were injected intravenously into Pan02 tumor-bearing mice and their blood clearance behaviors were investigated. As expected, PpIX underwent rapid blood clearance and there was little circulating PpIX at 0.5 h post-injection (Figure S14). However, PpIX-NLG-RGD NI was cleared much more slowly and a strong signal was still observed even after 6 h, suggesting its favorable pharmacokinetics.

To further confirm RGD-mediated active tumor targeting *in vivo*, the bio-distribution of PpIX-NLG-RAD NI and PpIX-NLG-RGD NI in tumors and major organs was revealed by fluorescence imaging (Figure S15). At 24 h post-injection, the tumor from PpIX-NLG-RAD NI treated mouse exhibited a higher fluorescence intensity than any other organ, suggesting its preferential tumor accumulation *via* the enhanced permeability and retention (EPR) effect.<sup>30-32</sup> Notably,

<sup>PpIX</sup>NLG-RGD NI treatment led to a much stronger fluorescence signal in tumor than its counterpart, proving its more effective tumor accumulation *via* active targeting. Moreover, the tumor still maintained a strong fluorescent signal even at 48 h post-injection of <sup>PpIX</sup>NLG-RGD NI, indicating its long-term tumor retention. In sharp contrast, PpIX showed a weak fluorescent signal in tumor after 24 h and a negligible fluorescent signal after 48 h due to the rapid metabolism and poor tumor accumulation of small molecules.

To prove that the admiring pharmacokinetics of NLG-RGD NI leads to the favorable pharmacological inhibition of IDO, we measured Kyn and Trp content in tumor after different treatment (Figure 3A). The ratio of Kyn to Trp decreased slightly at 24 h post-injection of NLG919 and then recovered at 48 h, suggesting a weak and transient inhibitory effect. In contrast, NLG-RGD NI exerted more potent suppression of Kyn conversion than NLG919 and exhibited sustained inhibition of intratumoral IDO activity over 48 h. Consistent with its inferior tumor accumulation and cellular uptake, the inhibitory effect of NLG-RAD NI was much weaker than NLG-RGD NI. We also examined the systemic IDO activity by measuring Kyn and Trp content in blood (Figure 3B). NLG919 dramatically reduced the ratio of Kyn to Trp in 24 h, indicating its potent inhibition of systemic IDO activity. Thanks to the controlled release of NLG919, both NLG-RAD NI and NLG-RGD NI showed moderate systemic IDO suppression in 48 h, implying the reduced risk of arousing immune disorders.<sup>33</sup> Together, these results suggest that NLG-RGD NI can significantly improve the bioavailability of NLG919 and preferentially inhibit intratumoral IDO activity in a sustained manner. It is worth mentioning that while NLG919 is orally administrated twice a day to maintain systemic IDO inhibition in clinical settings,<sup>17</sup> our improved IDO formulation may reduce the dose as well as frequency and still provide superior intratumoral IDO suppression.

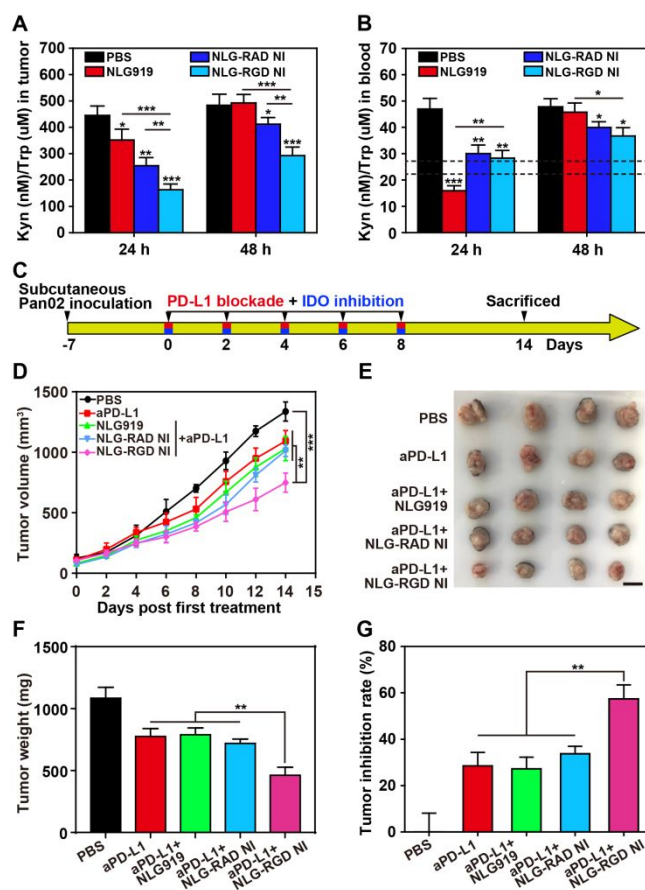


**Figure 3.** Combinatorial normalization immunotherapy using NLG-RGD NI and aPD-L1 in the subcutaneous Pan02 tumor model. (A) Kyn/Trp ratio in tumor. (B) Kyn/Trp ratio in blood. The dash lines indicate the range of Kyn/Trp ratio in healthy mice. (C) Scheme of combinatorial normalization immunotherapy. (D) Tumor growth curves. (E) Photograph of excised tumors. Scale bar, 1 cm. (F) Tumor weights. (G) Tumor inhibition rates. Mean  $\pm$  SD.,  $n = 4$ . \* $p < 0.05$ , \*\* $p < 0.01$ , \*\*\* $p < 0.001$ , one-way ANOVA.

**Dual-Blockade of IDO and PD-L1 for Combinatorial Normalization Immunotherapy.** Since IDO inhibition as a standalone therapeutic intervention has limited efficacy in preventing tumor progression,<sup>34</sup> considerable efforts have been made to investigate the combination therapy of immune checkpoint blockade and IDO inhibition.<sup>35</sup> So we first evaluated the ability of NLG-RGD NI to augment the efficacy of PD-L1 blockade immunotherapy in the subcutaneous Pan02 tumor model (Figure 3C). Single-agent aPD-L1 demonstrated a mild anti-tumor activity with an undesirable tumor inhibition rate (TIR) of 28.4% (Figure 3D-G). Surprisingly, when combined with NLG919, aPD-L1 did not further delay tumor growth (TIR = 27.2%). The insufficient IDO inhibition within tumor should be blamed for this, which could be the same reason for the recent failure of phase III ECHO-301 trial.<sup>36</sup> A similar result was observed when aPD-L1 was combined with NLG-RAD NI (TIR = 33.7%). However, NLG-RGD NI in combination with aPD-L1 dramatically boosted the therapeutic efficacy with an improved TIR of 57.4%, which is approximately two-fold higher than that of aPD-L1

monotherapy and other combinations. The superior anti-tumor efficacy of this combinatorial normalization immunotherapy was further confirmed in the orthotopic Pan02 tumor model with the highest TIR of 60.8% (Figure S16). Collectively, these results indicate that the robust and persistent inhibition of intratumoral IDO activity, which is only provided by NLG-RGD NI, is a prerequisite for greatly improving the anti-tumor response of PD-L1 blockade.

**Analysis of anti-tumor immune responses.** To elucidate the immunological mechanisms underlying the enhanced anti-tumor effect of this combinatorial therapy, we next analyzed tumor infiltrating immune cell populations using flow cytometry. Among all treatment groups, the combination of aPD-L1 and NLG-RGD NI resulted in the highest proportion of CD4<sup>+</sup> and CD8<sup>+</sup> T cells and interferon- $\gamma$  (IFN- $\gamma$ )-producing CD4<sup>+</sup> and CD8<sup>+</sup> T cells (Figure 4A-D and Figure S17 and S18). Moreover, compared to aPD-L1 monotherapy or other therapeutic combinations, the percentage of Treg (CD4<sup>+</sup>CD25<sup>+</sup>) cells dramatically decreased in aPD-L1 plus NLG-RGD NI group (Figure 4E and Figure S19). Interestingly, aPD-L1 plus NLG-RGD NI treatment also significantly increased the percentage of NK (CD49b<sup>+</sup>CD69<sup>+</sup>) cells (Figure 4F and Figure S20). NK cells also express PD-1 and are sensitive to tryptophan deficiency,<sup>37,38</sup> which can explain the enhanced NK cell response after this combinatorial therapy. Finally, intratumoral IFN- $\gamma$  and interleukin-2 (IL-2), two important indicators of T-cell activity and proliferation, were analyzed by enzyme-linked immunosorbent assay (ELISA). Both of them were found to be the highest in aPD-L1 plus NLG-RGD NI group (Figure 4G, H). These findings support that aPD-L1 plus NLG-RGD NI efficiently elicits anti-tumor immunity by enhancing the activation and survival of immune effector cells, and attenuating the accumulation immunosuppressive Treg cells. Similar anti-tumor immune responses were also revealed by flow cytometry analysis in the orthotopic Pan02 tumor mode (Figure S21).

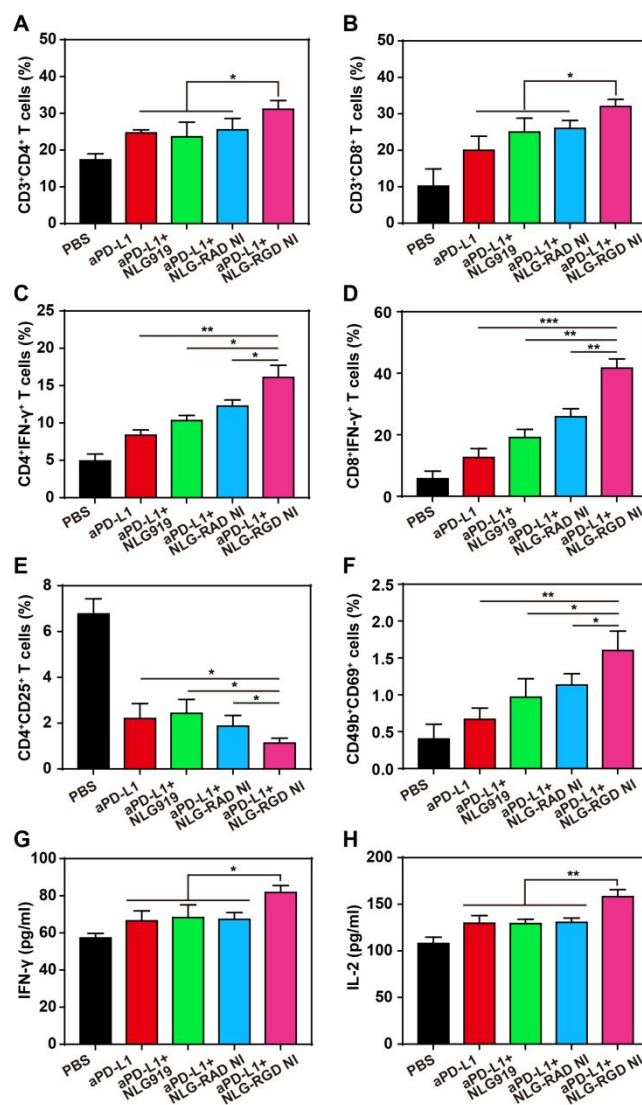


**Figure 4.** Analysis of anti-tumor immune responses in the subcutaneous Pan02 tumor model. (A) Percentage of CD4<sup>+</sup> T cells. (B) Percentage of CD8<sup>+</sup> T cells. (C) Percentage of IFN- $\gamma$ -producing CD4<sup>+</sup> T cells. (D) Percentage of IFN- $\gamma$ -producing CD8<sup>+</sup> T cells. (E) Percentage of Treg cells in CD4<sup>+</sup> T cells. (F) Percentage of NK cells in tumor. (G) Intratumoral IFN- $\gamma$ . (H) Intratumoral IL-2. Mean  $\pm$  SD., n = 4. \* $p$  < 0.05, \*\* $p$  < 0.01, \*\*\* $p$  < 0.001, one-way ANOVA.

During the treatment period, no obvious changes in mouse body weight were observed in any group (Figure S22). Hematoxylin and eosin (H&E) staining results revealed normal histological morphologies in major organs of all treated groups (Figure S23). However, serum biochemical analysis indicated that aPD-L1 plus NLG919 affected liver function of the treated mice (Figure S24), which is a typical adverse effect of NLG919.<sup>16</sup> In contrast, other therapeutic combinations demonstrated no noticeable changes of serum biomarkers. Together, these results suggest the good tolerance of NLG-RGD NI in combination with aPD-L1.

## CONCLUSION

In summary, we report a modularly designed and self-assembled IDO nanoinhibitor. *In vivo* studies demonstrate that it achieves potent and persistent inhibition of intratumoral IDO pathway due to its preferential tumor accumulation and sustained drug release. Significantly, this nanoinhibitor boosts the anti-tumor immune response of PD-L1 blockade by increasing immune effector cells and reducing immunosuppressive cells. Therefore, it holds great promise to serve as a powerful combination partner to enhance the efficacy of current immune checkpoint blockade-based immunotherapies by combinatorial normalization of the immunosuppressive TME.

## ASSOCIATED CONTENT

### Supporting Information

The Supporting Information is available free of charge on the ACS Publications website at DOI:

Materials, methods, <sup>1</sup>H-NMR analysis, HPLC analysis, MALDI-TOF-MS analysis, CMC measurement, acidic pH-triggered disassembly, cell viability, cellular uptake, pharmacokinetics, bio-distribution, flow cytometry analysis and serum biochemical analysis. (PDF)

## AUTHOR INFORMATION

### Corresponding Author

\*E-mail: niegj@nanocr.cn

\*E-mail: liyy@nanocr.cn

### Author Contributions

#These authors contributed equally to this work.

### Notes

The authors declare no competing financial interest.

## ACKNOWLEDGMENT

This work was supported by the grants from National Basic Research Plan of China (2018YFA0208900, 2016YFA0201600), National Natural Science Foundation of China (31571021), Innovation Group of the National Natural Science Foundation of China (11621505), Frontier Research Program of the Chinese Academy of Sciences (QYZDJ-SSW-SLH022), and the Key Laboratory of Biomedical Effects of Nanomaterials and Nanosafety, CAS.

## REFERENCES

1. Chen, D. S.; Mellman, I. Oncology meets immunology: the cancer-immunity cycle. *Immunity* **2013**, *39*, 1-10.
2. Topalian, S. L.; Drake, C. G.; Pardoll, D. M. Immune checkpoint blockade: A common denominator approach to cancer therapy. *Cancer Cell* **2015**, *27*, 450-461.
3. Ribas, A.; Wolchok, J. D. Cancer immunotherapy using checkpoint blockade. *Science* **2018**, *359*, 1350-1355.
4. Zou, W. P.; Chen, L. P. Inhibitory B7-family molecules in the tumour microenvironment. *Nat. Rev. Immunol.* **2008**, *8*, 467-477.
5. Freeman, G. J.; Long, A. J.; Iwai, Y.; Bourque, K.; Chernova, T.; Nishimura, H.; Fitz, L. J.; Malenkovich, N.; Okazaki, T.; Byrne, M. C.; Horton, H. F.; Fouser, L.; Carter, L.; Ling, V.; Bowman, M. R.; Carreno, B. M.; Collins, M.; Wood, C. R.; Honjo,

T. Engagement of the PD-1 immunoinhibitory receptor by a novel B7 family member leads to negative regulation of lymphocyte activation. *J. Exp. Med.* **2000**, *192*, 1027-1034.

6. Sanmamed, M. F.; Chen, L. P. A paradigm shift in cancer immunotherapy: From enhancement to normalization. *Cell* **2018**, *175*, 313-326.

7. Zou, W. P.; Wolchok, J. D.; Chen, L. P. PD-L1 (B7-H1) and PD-1 pathway blockade for cancer therapy: Mechanisms, response biomarkers, and combinations. *Sci. Transl. Med.* **2016**, *8*, 328rv324.

8. Brahmer, J. R.; Tykodi, S. S.; Chow, L. Q. M.; Hwu, W. J.; Topalian, S. L.; Hwu, P.; Drake, C. G.; Camacho, L. H.; Kauh, J.; Odunsi, K.; Pitot, H. C.; Hamid, O.; Bhatia, S.; Martins, R.; Eaton, K.; Chen, S. M.; Salay, T. M.; Alaparthi, S.; Grosso, J. F.; Korman, A. J.; Parker, S. M.; Agrawal, S.; Goldberg, S. M.; Pardoll, D. M.; Gupta, A.; Wigginton, J. M. Safety and activity of anti-PD-L1 antibody in patients with advanced cancer. *N. Engl. J. Med.* **2012**, *366*, 2455-2465.

9. Molinier-Frenkel, V.; Castellano, F. Immunosuppressive enzymes in the tumor microenvironment. *FEBS Lett.* **2017**, *591*, 3135-3157.

10. Chen, Y. C.; Sun, J. J.; Huang, Y. X.; Lu, B. F.; Li, S. Improved cancer immunotherapy via optimal co-delivery of chemotherapeutic and immunomodulatory agents. *Mol. Pharm.* **2018**, *15*, 5162-5173.

11. Smyth, M. J.; Ngiow, S. F.; Ribas, A.; Teng, M. W. Combination cancer immunotherapies tailored to the tumour microenvironment. *Nat. Rev. Clin. Oncol.* **2016**, *13*, 143-158.

12. Zappasodi, R.; Merghoub, T.; Wolchok, J. D. Emerging concepts for immune checkpoint blockade-based combination therapies. *Cancer Cell* **2018**, *34*, 690.

13. Yu, S.; Wang, C.; Yu, J.; Wang, J.; Lu, Y.; Zhang, Y.; Zhang, X.; Hu, Q.; Sun, W.; He, C.; Chen, X.; Gu, Z. Injectable bioresponsive gel depot for enhanced immune checkpoint blockade. *Adv. Mater.* **2018**, *30*, e1801527.

14. Ruan, H.; Bu, L.; Hu, Q.; Cheng, H.; Lu, W.; Gu, Z. Strategies of combination drug delivery for immune checkpoint blockades. *Adv. Healthc. Mater.* **2019**, *8*, e1801099.

15. Prendergast, G. C.; Malachowski, W. P.; DuHadaway, J. B.; Muller, A. J. Discovery of IDO1 inhibitors: From bench to bedside. *Cancer Res.* **2017**, *77*, 6795-6811.

16. Cheong, J. E.; Sun, L. Targeting the IDO1/TDO2-KYN-AhR pathway for cancer immunotherapy - challenges and opportunities. *Trends Pharmacol. Sci.* **2018**, *39*, 307-325.

17. Nayak-Kapoor, A.; Hao, Z.; Sadek, R.; Dobbins, R.; Marshall, L.; Vahanian, N. N.; Jay Ramsey, W.; Kennedy, E.; Mautino, M. R.; Link, C. J.; Lin, R. S.; Royer-Joo, S.; Liang, X.; Salphati, L.; Morrissey, K. M.; Mahrus, S.; McCall, B.; Pirzkall, A.; Munn, D. H.; Janik, J. E.; Khleif, S. N. Phase Ia study of the indoleamine 2,3-dioxygenase 1 (IDO1) inhibitor navoximod (GDC-0919) in patients with recurrent advanced solid tumors. *J. Immunother. cancer* **2018**, *6*, 61.

18. Munn, D. H.; Mellor, A. L. IDO in the tumor microenvironment: Inflammation, counter-regulation, and tolerance. *Trends Immunol.* **2016**, *37*, 193-207.

19. Uyttenhove, C.; Pilotte, L.; Theate, I.; Stroobant, V.; Colau, D.; Parmentier, N.; Boon, T.; Van den Eynde, B. J. Evidence for a tumoral immune resistance mechanism based on tryptophan degradation by indoleamine 2,3-dioxygenase. *Nat. Med.* **2003**, *9*, 1269-1274.

20. Munn, D. H.; Sharma, M. D.; Baban, B.; Harding, H. P.; Zhang, Y.; Ron, D.; Mellor, A. L. GCN2 kinase in T cells mediates proliferative arrest and anergy induction in response to indoleamine 2,3-dioxygenase. *Immunity* **2005**, *22*, 633-642.

21. Chen, Y. C.; Xia, R.; Huang, Y. X.; Zhao, W. C.; Li, J.; Zhang, X. L.; Wang, P. C.; Venkataramanan, R.; Fan, J.; Xie, W.; Ma, X. C.; Lu, B. F.; Li, S. An immunostimulatory dual-functional nanocarrier that improves cancer immunochemotherapy. *Nat. Commun.* **2016**, *7*, 13443.
22. Sun, J. J.; Chen, Y. C.; Huang, Y. X.; Zhao, W. C.; Liu, Y. H.; Venkataramanan, R.; Lu, B. F.; Li, S. Programmable co-delivery of the immune checkpoint inhibitor NLG919 and chemotherapeutic doxorubicin via a redox-responsive immunostimulatory polymeric prodrug carrier. *Acta Pharmacol. Sin.* **2017**, *38*, 823-834.
23. Zhai, Q. Y.; Chen, Y. C.; Xu, J. N.; Huang, Y. X.; Sun, J. J.; Liu, Y. H.; Zhang, X. L.; Li, S.; Tang, S. Q. Lymphoma immunochemotherapy: Targeted delivery of doxorubicin via a dual functional nanocarrier. *Mol. Pharm.* **2017**, *14*, 3888-3895.
24. Li, J.; Cui, D.; Huang, J.; He, S.; Yang, Z.; Zhang, Y.; Luo, Y.; Pu, K. Organic semiconducting pro-nanostimulants for near-infrared photoactivatable cancer immunotherapy. *Angew. Chem. Int. Ed.* **2019**, *58*, 2-10.
25. Li, S.; Zou, Q.; Li, Y.; Yuan, C.; Xing, R.; Yan, X. Smart peptide-based supramolecular photodynamic metallo-nanodrugs designed by multicomponent coordination self-assembly. *J. Am. Chem. Soc.* **2018**, *140*, 10794-10802.
26. Cheng, K. M.; Ding, Y. P.; Zhao, Y.; Ye, S. F.; Zhao, X.; Zhang, Y. L.; Ji, T. J.; Wu, H. H.; Wang, B.; Anderson, G. J.; Ren, L.; Nie, G. J. Sequentially responsive therapeutic peptide assembling nanoparticles for dual-targeted cancer immunotherapy. *Nano Lett.* **2018**, *18*, 3250-3258.
27. Qiu, N. S.; Liu, X. R.; Zhong, Y.; Zhou, Z. X.; Piao, Y.; Miao, L.; Zhang, Q. Z.; Tang, J. B.; Huang, L.; Shen, Y. Q. Esterase-activated charge-reversal polymer for fibroblast-exempt cancer gene therapy. *Adv. Mater.* **2016**, *28*, 10613-10622.
28. Oba, M.; Aoyagi, K.; Miyata, K.; Matsumoto, Y.; Itaka, K.; Nishiyama, N.; Yamasaki, Y.; Koyama, H.; Kataoka, K. Polyplex micelles with cyclic RGD peptide ligands and disulfide cross-links directing to the enhanced transfection via controlled intracellular trafficking. *Mol. Pharm.* **2008**, *5*, 1080-1092.
29. Han, K.; Zhang, J.; Zhang, W. Y.; Wang, S. B.; Wu, L. M.; Zhang, C.; Zhang, X. Z.; Han, H. Y. Tumor-triggered geometrical shape switch of chimeric peptide for enhanced in vivo tumor internalization and photodynamic therapy. *ACS Nano* **2017**, *11*, 3178-3188.
30. Maeda, H. The enhanced permeability and retention (EPR) effect in tumor vasculature: The key role of tumor-selective macromolecular drug targeting. *Adv. Enzyme Regul.* **2001**, *41*, 189-207.
31. Han, X.; Li, Y.; Xu, Y.; Zhao, X.; Zhang, Y.; Yang, X.; Wang, Y.; Zhao, R.; Anderson, G. J.; Zhao, Y.; Nie, G. Reversal of pancreatic desmoplasia by re-educating stellate cells with a tumour microenvironment-activated nanosystem. *Nat. Commun.* **2018**, *9*, 3390.
32. Han, X.; Xu, Y.; Li, Y.; Zhao, X.; Zhang, Y.; Min, H.; Qi, Y.; Anderson, G. J.; You, L.; Zhao, Y.; Nie, G. An extendable star-like nanoplatform for functional and anatomical imaging-guided photothermal oncotherapy. *ACS Nano* **2019**, *13*, 4379-4391.
33. Yi, Y. M.; Zhang, G.; Zeng, J.; Huang, S. C.; Li, L. L.; Fang, R.; Jiang, G. M.; Bu, X. Z.; Cai, S. H.; Du, J. A new tumor vaccine: FAPtau-MT elicits effective antitumor response by targeting indoleamine 2,3-dioxygenase in antigen presenting cells. *Cancer Biol. Ther.* **2011**, *11*, 866-873.
34. Li, F.; Zhang, R.; Li, S.; Liu, J. IDO1: An important immunotherapy target in cancer treatment. *Int. Immunopharmacol.* **2017**, *47*, 70-77.
35. Brochez, L.; Chevolet, I.; Kruse, V. The rationale of indoleamine 2,3-dioxygenase inhibition for cancer therapy. *Eur. J. Cancer* **2017**, *76*, 167-182.
36. Muller, A. J.; Manfredi, M. G.; Zakharia, Y.; Prendergast, G. C. Inhibiting IDO pathways to treat cancer: lessons from the ECHO-301 trial and beyond. *Semin. Immunopathol.* **2019**, *41*, 41-48.
37. Hsu, J.; Hodgins, J. J.; Marathe, M.; Nicolai, C. J.; Bourgeois-Daigneault, M. C.; Trevino, T. N.; Azimi, C. S.; Scheer, A. K.; Randolph, H. E.; Thompson, T. W.; Zhang, L.; Iannello, A.; Mathur, N.; Jardine, K. E.; Kirn, G. A.; Bell, J. C.; McBurney, M. W.; Raulet, D. H.; Ardolino, M. Contribution of NK cells to immunotherapy mediated by PD-1/PD-L1 blockade. *J. Clin. Invest.* **2018**, *128*, 4654-4668.
38. Frumento, G.; Rotondo, R.; Tonetti, M.; Damonte, G.; Benatti, U.; Ferrara, G. B. Tryptophan-derived catabolites are responsible for inhibition of T and natural killer cell proliferation induced by indoleamine 2,3-dioxygenase. *J. Exp. Med.* **2002**, *196*, 459-468.

## Table of contents (TOC) graphic

